ACS APPLIED MATERIALS & INTERFACES

Research Article

www.acsami.org

Hybrid Wood Materials with Magnetic Anisotropy Dictated by the Hierarchical Cell Structure

Vivian Merk,[†,‡] Munish Chanana,*[,†,∥] Notburga Gierlinger,[†,‡] Ann M. Hirt,[§] and Ingo Burgert*[,†,‡]

[†]Institute for Building Materials (IfB), Wood Materials Science, ETH Zürich, Stefano-Franscini-Platz 3, 8093 Zürich, Switzerland

[‡]Applied Wood Materials Laboratory, Empa - Swiss Federal Laboratories for Material Testing and Research, 8600 Dübendorf, Switzerland

[∥]Physical Chemistry II, University of Bayreuth, Universitätsstr. 30, 95447 Bayreuth, Germany

[§]Institute for Geophysics, Earth and Planetary Magnetism, ETH Zürich, Sonneggstrasse 5, 8092 Zürich, Switzerland

Supporting Information

ABSTRACT: Anisotropic and hierarchical structures are bound in nature and highly desired in engineered materials, due to their outstanding functions and performance. Mimicking such natural features with synthetic materials and methods has been a highly active area of research in the last decades. Unlike these methods, we use the native biomaterial wood, with its intrinsic anisotropy and hierarchy as a directional scaffold for the incorporation of magnetic nanoparticles inside the wood material. Nanocrystalline iron oxide particles were synthesized in situ via coprecipitation of ferric and ferrous ions within the interconnected pore network of bulk wood. Imaging with low-vacuum and cryogenic electron microscopy as well as spectral Raman mapping revealed layered nanosize particles firmly attached to the inner surface of the wood cell walls. The mineralogy of iron oxide was identified by XRD powder diffraction and Raman spectroscopy as a mixture of the spinel phases magnetite and maghemite. The intrinsic structural architecture of native wood entails a three-dimensional assembly of the colloidal iron oxide which results in direction-dependent magnetic features of the wood−mineral hybrid material. This superinduced magnetic anisotropy, as quantified by direction-dependent magnetic hysteresis loops and low-field susceptibility tensors, allows for directional lift, drag, alignment, (re)orientation, and actuation, and opens up novel applications of the natural resource wood.

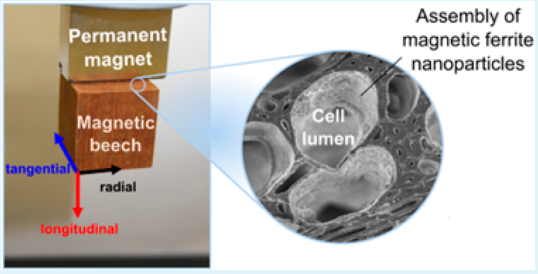

KEYWORDS: *wood modification, structural hierarchy, iron oxide nanoparticles, coprecipitation, magnetic anisotropy, hybrid material actuation*

INTRODUCTION

On the basis of organic−mineral composites natural hybrid materials are known for excellent mechanical properties and sophisticated coalescence of complex functionality.[1−5] A key feature of many biological materials is their inherent hierarchical structure, which allows embedded material to take on a distribution that represents the structure of the original material.[6] This structure then leads to directionally dependent functions. Nature is rich in such anisotropic materials including not only inorganic (crystals−quartz) and organic (fibers−collagen, cellulose) materials, but also biological structures and architectures that give rise to sophisticated functions, such as water repellency (spider silk[71]), brilliant colors (butterfly wings),[8] locomotion (snake skin),[9] drag and turbulence reduction (shark skin),[10] and adapted mechanical properties (wood).[11,12] Understanding and capturing the underlying principles for the design of biomimetic and engineered materials may open new perspectives in the field of materials science toward sustainable and renewable materials.[13]

Mimicking such natural features with synthetic materials and methods has been a highly active area of research for the last decades. Much effort has been devoted to creating functional anisotropic materials by organizing micro- and nanoscaled building blocks into superlattice assemblies and hierarchical or terminal structures in order to produce devices that feature direction-dependent properties. Common methods for creating such structures are bottom up approaches, such as self-assembly methods, stepwise layer-by-layer deposition[14] and (micro-contact) printing, or top-down methods such as lithographic techniques,[15−17] which are very arduous, time-consuming, generally small in scale (usually in nano or microscale), and highly expensive in terms of up-scaled fabrication. Unlike these methods, we foster the concept of using a native biomaterial with its hierarchical structure and intrinsic anisotropy as a directional scaffold to incorporate in situ functional nanomaterials to develop sophisticated materials ranging from micro up

Received: April 10, 2014
Accepted: May 29, 2014
Published: May 29, 2014

   dx.doi.org/10.1021/am5021793 | ACS Appl. Mater. Interfaces 2014, 6, 9760−9767

to a few meter scales. Cellulosic materials[18] with embedded magnetic properties have been developed ranging from lignocellulosic pulp[19−21] over cellulose fibers[22,23] to highly processed bacterial cellulose fibrils.[24,25] In contrast to the above-mentioned fiber-based composites wood possesses a sophisticated cell wall anatomy allowing for three-dimensional nanoparticle assembly on a higher degree of hierarchy.[26] The dominating directionality is implemented at the level of fibrous elongated cells, which are oriented parallel to the stem axis (longitudinal) and consist of cell walls made up of parallel aligned cellulose fibrils embedded in a matrix of hemicelluloses and lignin.[27] The dominating functions of wood in the tree are mechanical support and conduction of water resulting in an excellent lightweight engineering material and providing an anisotropic hierarchical scaffold for further functionalization. Using a nanotemplating approach,[28,29] the anisotropic nature of plant tissues, e.g., wood[30−32] or leaves,[33] has been replicated in porous magnetic ceramics up to the submicrometer scale, but without retaining the functionalized bulk wood structure.

Oka et al. fabricated magnetic wood by loading wood fiber boards, coatings, and impregnated veneers with commercial magnetic fluids.[18,34] Cedar sapwood and heartwood exhibited anisotropic magnetic response after being pressure-impregnated with aqueous magnetite particle dispersions. The authors suggested that this result originated from the wood structure, but did not further examine the effects in terms of colloidal features, such as spatial distribution, size, aggregation state, surface properties, penetration depth, and leachability of the incorporated particles.[18]

Here, we report on a magnetic wood−nanocomposite hybrid material, which is not only directional in terms of structural and mechanical properties, but also features magnetic anisotropy dictated by the intrinsic wood architecture. Using an in situ fabrication approach we were able to control the final iron oxide content through in-depth penetration of ferric and ferrous ions and ferrite precipitation within hardwood and softwood matrices. By exploiting the hierarchical superstructure of wood as a template for self-assembled ferrite nanoparticles, anisotropic organic−inorganic hybrid materials can be produced that are not limited in shape and size.

EXPERIMENTAL SECTION

Chemical Synthesis. Magnetic wood was prepared from cubic samples ($4 \times 4 \times 4$ mm^3, $10 \times 10 \times 10$ mm^3, $20 \times 20 \times 20$ mm^3) of Norway spruce (*Picea abies*) and European beech (*Fagus sylvatica*) via a simple chemical coprecipitation of ferric and ferrous chloride upon the addition of aqueous ammonia. Prior to chemical modification the samples were dried in a BINDER vacuum oven at 65 °C for 48 h. Magnetic wood was fabricated by chemical coprecipitation of ferric and ferrous chloride with a fixed molar ratio of 2:1 with a concentration of 0.165 mol L^{-1}, 0.330 mol L^{-1}, 0.660 mol L^{-1}, 0.990 mol L^{-1}, and 1.320 mol LL^{-1} ferric chloride. The excess amount of aqueous ammonia solution was 1 mL per 0.165 mol $FeCl_3$. The samples were entirely incubated in the reaction solution for 5 h (4 mm sample size) and 6.3 h (10 mm sample size) and vacuum-impregnated at least three times to allow for in-depth diffusion into the porous wood structure. After rapid addition of excess ammonia, the reaction solution was stirred for 1 h. After the treatment, the samples were removed from the beaker and washed with deionized water until reaching neutral pH. The modified wood cubes were dried in the vacuum oven at 65 °C for 48 h followed by immersion in water for 5 days. During the washing process, the washing water was changed twice a day. After washing, the magnetic wood samples were dried again for 48 h in the vacuum oven. The mass change for 4-mm-sized and 10-mm-sized beech and spruce samples are shown in SI Figure S1a and Figure S1b as a function of the precursor concentration.

$FeCl_3$·6H2O, $FeCl_2$·4H_2O, ammonium hydroxide solution (≥25%), and hydrochloric acid (≥37%) were purchased from Sigma-Aldrich.

Material Characterization. *Light Microscopy.* Light microscopy was performed with a Leica M165C stereomicroscope (1.0× objective) coupled to a Basler GigE Vision camera. Images were recorded with a control plugin (PHASE GmbH) for the program ImageJ 1.47c.

ESEM-EDX. Environmental scanning electron microscopy (ESEM) in the low-vacuum mode was carried out on a FEI Quanta 200 3D coupled to an EDAX energy-dispersive X-ray spectrometer.

Cryo-SEM. High resolution cryogenic scanning electron images were obtained with a Zeiss Leo Gemini 1530 FEG (field emission gun) equipped with an secondary electron in-lens detector and driven at an accelerating voltage of 5.0 kV. Exemplary magnetic beech and spruce specimens (0.333 mol L^{-1} Fe^{3+}, 0.165 mol L^{-1} Fe^{2+}) were freeze-fractured across the grain under liquid nitrogen; cross sections were prepared with a conventional rotary microtome, followed by W-sputtering of the specimen surface.

Raman Microscopy. For the Raman measurements cross sections (20−25 μm) of magnetic beech and spruce (0.330 mol L^{-1} Fe^{3+}, 0.165 mol L^{-1} Fe^{2+}) cut with a rotary microtome (Leica Ultracut, Germany)) were placed on a microscope slide with a drop of D_2O and sealed with a coverslip and nail polish to avoid evaporation. All Raman spectra were collected with a confocal Raman-microscope (Renishaw InVia) equipped with a Nd:YAG laser (λ = 532 nm), a 600 grooves/mm grating, and a 100× oil immersion objective (Nikon, NA = 1.4). The laser power was set to low values (1%) to avoid sample degradation due to intense laser excitation. In order to achieve good spectral quality nonetheless, it was necessary to prolong the acquisition time to 10 s. The pixel size of the spectroscopic Raman maps was 0.3 μm. The data were processed with the program Wire 3.4.

Vibrating Sample Magnetometry. Magnetic hysteresis curves of chemically modified wood cubes (edge length $d \approx 4$ mm) were determined with a MicroMag 3900 Vibrating Sample Magnetometer (Princeton Measurements Corporation) in a magnetic field ranging from −10 kOe to 10 kOe in 100 Oe steps and an averaging time of 100 ms.

Kappabridge. The bulk susceptibility and the anisotropy of low-field magnetic susceptibility were measured with a KLY-2 inductive susceptibility bridge (AGICO) by spinning a cubic wood specimen (edge length $d \approx 10$ mm) at a magnetic field of 200 A m^{-1} according to a static 15-position rotation scheme.[35,36] The samples were mounted so that the three orthogonal axes of the coordinate system were commensurate with the wood directions X_1 = tangential, X_2 = radial, and X_3 = longitudinal. Processing of the data and equal-area lower-hemisphere stereographic projections of the magnetic anisotropy tensors were made with the program Anisoft42 (AGICO).

Compression Perpendicular to the Grain. The compressive strength of magnetic spruce and beech compared to unmodified wood specimens of approximately 20 mm in height, width, and length was tested with a Zwick Roell Z010 (Zwick) testing machine with a 10 kN load cell in a standard climate (20 °C, 65% relative humidity) in the tangential direction. The deformation was determined in a contact-free way by using a videoextensometer system (CCD camera) and a pair of parallel paper stripes attached to the cross-sectional area of the wood block revealing the displacement upon compression. The data were processed with the program TestxpertII.

X-ray Powder Diffraction. XRD diffraction patterns were recorded for magnetic beech and spruce (0.330 mol L^{-1} Fe^{3+}, 0.165 mol L^{-1} Fe^{2+} precursor concentration) using a Panalytical X'Pert PRO diffractometer equipped with a flat-disk sample holder and a copper X-ray source in a $2\Theta = 5-80°$ range with a counting time of 500 s.

RESULTS AND DISCUSSION

The iron oxides magnetite (Fe_3O_4) and maghemite (γ-Fe_2O_3) are two of the most common magnetic minerals in nature[37] and can be easily synthesized in situ[38] inside the bulk wood by

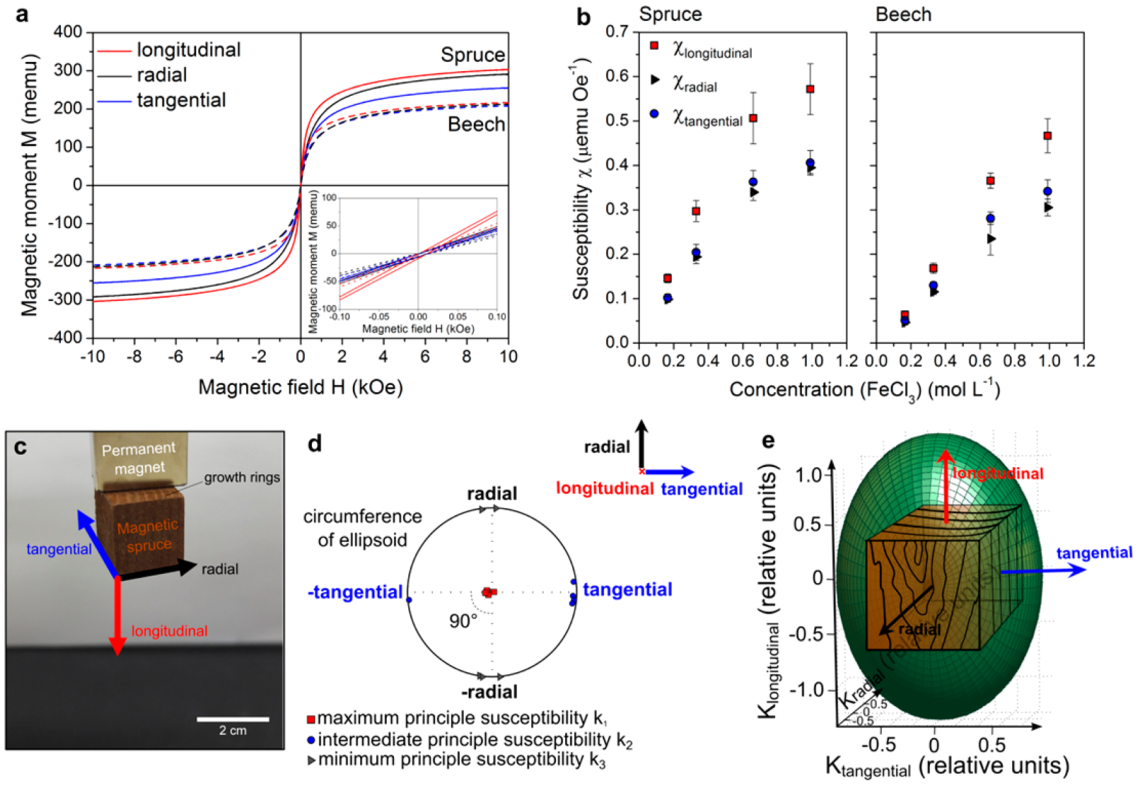

Figure 1. Magnetic characterization of common wood species via hysteresis curves and low-field susceptibility tensors. (a) Representative magnetic hysteresis curves in three wood directions of spruce (solid lined) and beech wood (dashed lines). (b) Magnetic susceptibility at low fields depends on the species, growth direction, and iron oxide content (given in precursor concentration): First-order derivative of hysteresis curves of magnetic spruce and beech at 100 Oe representing the directional low-field magnetic susceptibility. (c) Lifting of magnetic spruce specimen with a permanent magnet along the orthotropic longitudinal direction. (d) Equal-area lower hemisphere projection of the low-field anisotropy of magnetic susceptibility of spruce prepared with 0.330 mol L^{-1} Fe^{3+} and 0.165 mol L^{-1} Fe^{2+}. (e) Anisotropy of low-field magnetic susceptibility of magnetic spruce is visualized by an ellipsoid dependent on the wood directionality. As shown, the longest ellipsoid axis coincides with the longitudinal wood direction.

classical coprecipitation of ferric and ferrous salts in aqueous media with alkaline solutions.[39] The resulting samples of the magnetic wood material are uniformly rust or dark brown in color, indicating homogeneous modification of the wood blocks throughout the sample (see Figure S1d in Supporting Information (SI) − 2 cm blocks cut in the middle). The synthesized ferric oxides are small, but their magnetic properties reflect multidomain particles, and only carry a net magnetization in the presence of an external field (Figure 1a). When a magnetic field is applied, the samples are attracted to the magnet.

As the magnetic properties are dictated by the intrinsic cell structure of the wood material, it is most likely that the directionality of magnetic properties (magnetic susceptibility, magnetization saturation, etc.) also depends on the wood species, since different species exhibit different cell structure (Figure 1a and b). The low-field regime of the magnetic hysteresis curve (Figure 1b) is sensitive to the ferromagnetic fraction and commensurate to the iron ion precursor concentration and the gravimetrically determined iron oxide content (SI Figure S1a,b), e.g., 8 ± 1 wt% (spruce) or 7 ± 1 wt % (beech) at 0.990 mol L^{-1} Fe^{3+} and 0.495 mol L^{-1} Fe^{2+}. Thus, magnetic functionalities are bestowed on wood with only slightly increased density. As illustrated in Figure 1c, the magnetization can easily be probed by lifting up a magnetic wood block with a permanent magnet. This phenomenon is clearly observed in the rotational movement of magnetic spruce and beech in a magnetic field, being more pronounced in spruce than in beech (SI Videos V1−2). Our observation is confirmed by low-field susceptibility measurements of solid spruce and beech with an inductive susceptibility bridge. Magnetic susceptibility measurements clearly reveal the anisotropic nature of the hybrid material which is dictated by the bulk wood template. The anisotropic behavior of the magnetic wood blocks can be quantified by the direction dependent low-field magnetic susceptibility measurements (Figure 1d) and visualized by a 3D ellipsoid dependent on the wood directionality (Figure 1e). The stereographs project the magnetic susceptibility tensor onto a unit sphere in order to envisage the orientation of the principal susceptibilities $K_1 \geq K_2 \geq K_3$ and their orientation to each other in a drawing plane. The significantly higher value of K in the longitudinal wood direction can be explained by a lower barrier of domain reorientation as observed in thin magnetic films.[40,41] As shown in Figure 1e, the longest ellipsoid axis coincides with the longitudinal wood direction, which corresponds to the maximum principal susceptibility of the magnetic anisotropy tensor. The degree of magnetic anisotropy is characterized the ratio of the maximum to minimum principal susceptibilities,[42] namely, 1.77 for spruce and 1.70 for beech at an intermediate precursor concentration.

Electron microscopy and Raman spectroscopy were used to structurally and chemically examine the composite and to assign the anisotropy to the relevant hierarchical levels of the

dx.doi.org/10.1021/am5021793 | ACS Appl. Mater. Interfaces 2014, 6, 9760−9767

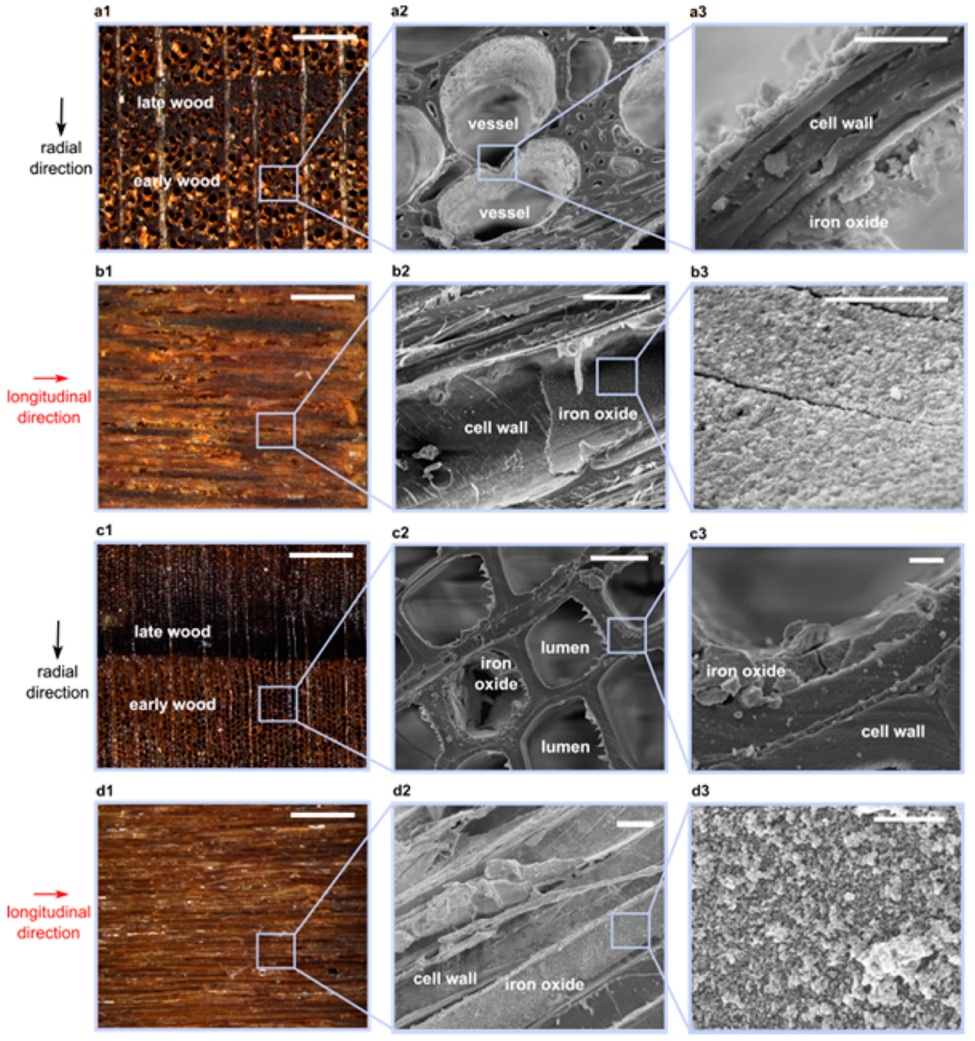

Figure 2. Light microscopy and cryogenic scanning electron microscopy collected in the secondary-electron mode showing microtome cross sections of beech (a) and spruce (c) and layered structures of iron oxide nanoparticles embedded in magnetic wood cut under ambient conditions (b1 and d1) or freeze-fractured under liquid nitrogen along the grain (b2, b3, d2, d3). All samples had been sputtered with tungsten prior to the SEM measurements. The scale bars correspond to 500 μm (a1, b1, c1, d1), 20 μm (a2, b2, c2, d2), and 2 μm (a3, b3, c3, d3).

biomaterial. The modified wood samples keep their lightweight character and low density (see also Figure S1a-b, SI), since the treatment only results in a thin-layer deposit at the inner cell surfaces and not in a simple lumen filling. Details of the covering of the inner surface of cell walls in bulk wood samples with a compact thin layer of iron oxide nanoparticles can be seen in Figure 2. Importantly, the modified wood samples show besides the low density also similar mechanical properties to native wood (see Figure S1c in SI) confirming that the process of embedding iron oxide nanoparticles does not harm the wood structure and intrinsic properties of wood are retained after modification.

Low-vacuum scanning electron microscopy (Figure S5, SI), light microscopy and cryogenic scanning electron microscopy (Figure 2) images of cross sections of both wood species illustrate the formation of thin layers of homogeneously dispersed ferric oxides in the lumina of the axially oriented structural wood elements.

At the low magnification (Figure 2 a2, b2, c2, and d2) the magnetic particle layers are particularly visible in the luminous vessels of the beech wood. Higher magnifications (Figure 2 a3 and c3) reveal a ~1−2-μm-thick and densely packed layer of iron oxide nanoparticles covering the inner surface of the cell wall of a tracheid. Cryo-SEM images of freeze-fractured beech wood at a higher magnification (Figure 2 b3 and d3) show nanoparticle aggregates of several tens of nanometers. According to FE-SEM, the colloidal assembly is constituted of nanoparticle grains in a size range of 22 ± 7 nm (beech) and 21 ± 6 nm (spruce) (see Figure S6−7, SI). In order to determine the crystallite sizes of Fe_3O_4/γ-Fe_2O_3, X-ray powder diffraction patterns of the wood hybrid material were recorded (Figure S8 a,b, SI). However, the signal (iron oxide, (440)) to background (wood) ratio was too low, due to the relatively low concentration of the inorganic material in the wood material. Therefore, an estimation of the crystallite size by using the Scherrer equation becomes vague. Nevertheless, the magnetization saturation measurements and the FE-SEM measurements indicate nanoscaled particles in the wood material. This inorganic network of particle aggregates seems to be more compact in spruce than in beech, which suggests that the varying degree of flocculation influences the magnetic coupling, for instance, ordering of magnetic moments in linear chains. Remarkably, the ultrafine particles remain immobilized in the wood superstructure even after immersion in water (washing

dx.doi.org/10.1021/am5021793 | ACS Appl. Mater. Interfaces 2014, 6, 9760−9767

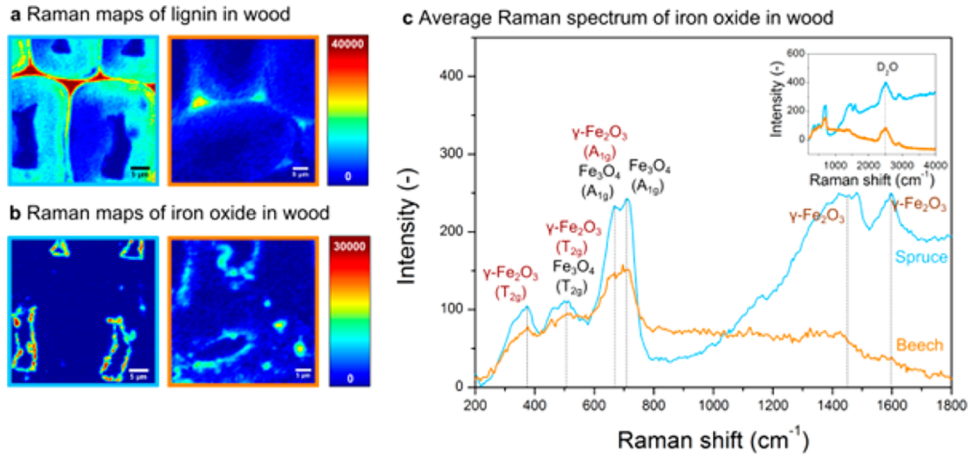

Figure 3. Raman spectroscopic microscopy of magnetic wood. The scattered light intensity measured in arbitrary cts (counts) units is visualized as color gradings. (a) Raman spectroscopic map showing distribution of the aromatic cell wall polymer lignin in spruce (blue frame) and beech (orange frame) latewood by integrating |1707−1540 cm^{-1}|. (b) Colloidal iron oxide, namely, magnetite Fe_3O_4 and γ-Fe_2O_3 seems to be mainly attached to the inner lumina walls of spruce and beech latewood imaged by integration of |825−566 cm^{-1}|. (c) Average Raman spectrum of iron oxide in spruce (blue curve) and beech (orange curve). (Inset) Survey spectrum in the range of |4000−200 cm^{-1}|.

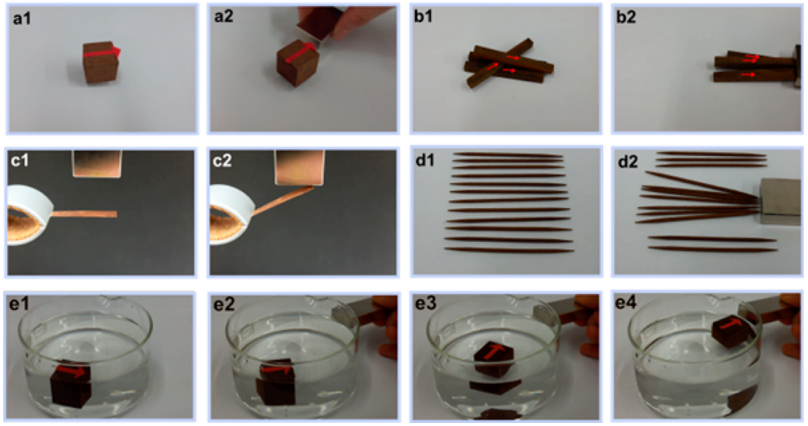

Figure 4. Magnetic wood samples of a common wood species, spruce and beech, under the influence of an external magnet (related videos in Supporting Information). (a1-a2) Flipping of a magnetic wood block mounted on a rotary, orienting itself with the wood fiber (longitudinal) direction parallel to the magnetic flux (see SI Video V1a-b). (b1-b2) Parallel alignment of wooden sticks in longitudinal direction (indicated by red arrows) (see SI Video V3). (c1-c2) Actuation of magnetic spruce platelet (see SI Video V4). (d1-d2) Alignment of magnetic tooth sticks along the magnetic flux lines (see SI Video V5). (e) Due to the low specific density magnetic wood floats on water and can be influenced by a magnetic field. (e1-e2) The floating specimen first orients along the wood fiber (longitudinal) direction (indicated by the red arrow) and moves toward the magnet (e3-e4) (see SI Video V6).

process) for 5 days indicating a tight interaction between the inorganic nanoparticles and the wood matrix which allows for eco-friendly applications indoors and outdoors. Harsh pH conditions during the synthesis, namely, pH < 3 during impregnation with $FeCl_3/FeCl_2$, pH > 12 after addition of aqueous ammonia, are likely to affect the organic tissue detrimentally, since dilute hydrochloric acid is known to hydrolyze carbohydrates.[43] Fragmentation reactions of aromatic lignin have been reported in alkaline media.[44] However, since the modified wood samples show similar mechanical properties to native wood (see Figure S1c in SI) it seems that the acidic and basic conditions in the process do not harm the wood structure.

XRD powder diffraction (Figure S8a,b, SI) gives evidence of nanocrystalline phases of magnetite and maghemite, but relies on the crystallinity of the minerals and renders the distinction between the two ferromagnetic spinel phases difficult.[45]

Therefore, Raman spectroscopic mapping was applied to the hybrid material to identify the composition of the inorganic phase in the wood matrix (inset Figure 3a and b) and to gain further information on the spatial distribution of colloidal iron oxide in the wood tissues. Spectral mapping of thin wood cross sections yields the distribution of the aromatic cell-wall polymer lignin and embedded nanocrystalline iron oxide (Figure 3a and b). In confirmation with the electron microscopic results, colloidal iron oxide is predominantly detected at the inner part of the lumina walls, hence it is likely that the tubular wood microarchitecture facilitates the highly anisotropic magnetic response.

The positions of the active Raman bands (Figure 3c) are sufficiently different to distinguish between iron oxide or oxyhydroxide[46,47] and the organic wood components (cellulose, hemicellulose, and lignin). Since iron oxides are highly vulnerable to irradiation-induced phase changes[48] the laser power was reduced to a minimum value, but peak integration

dx.doi.org/10.1021/am5021793 | ACS Appl. Mater. Interfaces 2014, 6, 9760−9767

time was extended to increase the signal-to-noise ratio. Average Raman spectra were obtained from of the FeO_x phase incorporated into spruce and beech (Figure 3c). The Raman-active Fe−O bands demonstrate the predominance of the ferrimagnetic phases magnetite Fe_3O_4 and maghemite γ-Fe_2O_3.[49] Magnetite (Fe_3O_4) comprises two magnetic sublattices with the tetrahedral (A) sites occupied by Fe^{3+} cations and the octrahedral (B) sites occupied by Fe^{2+} and Fe^{3+} cations in a spinel structure.[49] Hence, the crystal structure of magnetite gives rise to five Raman-active bands, $3T_{2g}$, E_g, and A_{1g} modes.[46] The main peak at 667−668 cm^{-1} present in all collected spectra can be assigned unambiguously to A_{1g}, whereas broader bands are found around 512−539 cm^{-1} (T_{2g}) and 319−324 cm^{-1} (E_g)[37] in this study. Weaker T_{2g} modes of magnetite are expected between 450 and 500 cm^{-1},[50] which have indeed been detected in the ranges 450−461 cm^{-1} and 465−475 cm^{-1}.

The heterogeneity of the mineral phase has been assessed spectroscopically by comparing the relative peak area of the Raman bands arising from Fe_3O_4 or γ-Fe_2O_3. As an iron-deficient form of magnetite, maghemite γ-Fe_2O_3 possesses an inverse spinel crystal structure, in which 2 and 1/3 octahedral lattice sites of the unit cell remain vacant. At ambient conditions, magnetite is prone to oxidation to maghemite, and they are end-members of a solid solution series. Probably due to a low degree of crystallinity, the Raman spectrum of maghemite is characterized by broad and less well-defined three active phonon modes around 350 cm^{-1} (T_{2g}), 500 cm^{-1} (E_g), and 700 cm^{-1} (A_{1g}).[46,37,47] By comparing with reported spectra,[46,47] the scattering bands at 376−377 cm^{-1}, 497−503 cm^{-1}, 677−682 cm^{-1}, 706−719 cm^{-1}, and 1594−1604 cm^{-1} have been ascribed to maghemite. According to the results, the relative percentage of maghemite seems to be higher in spruce than in beech (data not shown).

Strikingly, when magnetic wood is approached by a permanent magnet either from the tangential or radial wood direction, the wood first flips over, orienting itself with the wood fiber (longitudinal) direction parallel to the magnetic field and then is attracted by the magnet (see Video V1 in SI ("Flipping wood blocks of spruce and beech")). Wood of various shapes and geometries can be actuated selectively from this one direction (longitudinal) under an applied magnetic field by inducing a magnetically controlled torque or rotation (Figure 4 and Videos V1, V2, V6 in SI). This behavior indicates that such magnetic wood blocks are magnetically anisotropic and display a magnetic easy axis.

In general, a magnetically anisotropic material aligns its magnetic moment with one of its easy axes (energetically favorable directions of the magnetization) and the direction of its intrinsic magnetic easy axis is firmly determined by the shape for strongly magnetic materials or the magnetocrystalline structure. It is not expected that the precipitated iron oxides have a strong shape anisotropy. Assembling and settling of magnetite and maghemite along the cell walls in the wood material, however, would lead to a higher magnetic susceptibility along the longitudinal growth direction in comparison to the tangential or radial directions, hence a distribution anisotropy.[51] For this reason, the wood block aligns with its longitudinal direction to the external magnetic field, displaying an apparent (magnetic) easy axis of the whole hybrid material along the longitudinal growth direction of wood and also a magnetic anisotropy in the same direction.

This principle enables the production of a variety of active wood elements that can be precisely actuated along the longitudinal axis of the wood. Since wood can be easily engineered in desired forms and shapes, any kind of complex structure can be designed and fabricated, both before and/or after iron oxide modification. The significant advantage of such a hybrid wood system over conventional polymer or fiber hybrid material systems is that the magnetic properties of the magnetic wood are fixed in longitudinal direction. This unique property of the magnetic wood material can be used to align and organize any jumble of hybrid materials, adding a further value and function to the versatility of wood. By way of example, applications related to induction heating,[52] electromagnetic wave absorption,[53−57] or actuation[34] have been proposed for magnetic wood based on Mn−Zn ferrites.

CONCLUSIONS

Iron oxide NPs were imbedded via simple in situ coprecipitation synthesis inside the cellular structure of wood, resulting into a highly sophisticated nanobiocomposite with pronounced anisotropic magnetic properties. Owing to the predominant direction of magnetization along the wood fibers (longitudinal) such magnetic devices can be selectively manipulated from this direction, simply with an external magnet and therefore perform complex movements such as lift, drag, flip, alignment, (re)orientation, and actuation. The magnetic anisotropy of the composite material is dictated by the intrinsic anisotropy of the wood material and originates from a homogeneous deposition of nanocrystalline ferrites along the inner cell walls of the wood scaffold. Importantly, such modified wood materials retain their natural properties such as mechanical stiffness, porosity, and low density, which in combination with magnetic functionalities give rise to advanced biobased engineering materials. In view of a practical application, this fabrication approach allows for easy processing, better handling, and upscaled production of magnetic wood elements of arbitrary shapes and sizes.

ASSOCIATED CONTENT

Supporting Information

Average mass gain of wood samples; stress−strain curves of compression tests; photograph of cut wood samples; hysteresis curves of magnetic spruce and beech; lower-hemisphere equal area projections of anisotropy of magnetic susceptibility data; saturation magnetization data; ESEM images and EDX point analyses; FE-SEM images of layered nanoparticle assemblies in high magnification; histograms of particle size distributions, X-ray diffraction spectra of magnetic beech and spruce. This material is available free of charge via the Internet at http://pubs.acs.org.

AUTHOR INFORMATION

Corresponding Authors

*E-mail: munish.chanana@uni-bayreuth.de.
*E-mail: iburgert@ethz.ch.

Notes

The authors declare no competing financial interest.

ACKNOWLEDGMENTS

We thank the Bundesamt für Umwelt (BAFU) and Lignum, Switzerland for the financial support of the Wood Materials Science group. We thank Hans-Peter Hächler for the technical

support during the magnetic measurements and Dr. Roger Wepf for the collection of cryo-SEM images (EMEZ, ETH Zürich).

REFERENCES

(1) Malvadkar, N. A.; Hancock, M. J.; Sekeroglu, K.; Dressick, W. J.; Demirel, M. C. An Engineered Anisotropic Nanofilm with Unidirectional Wetting Properties. *Nat. Mater.* **2010**, *9*, 1023−1028.
(2) Glotzer, S. C.; Solomon, M. J. Anisotropy of Building Blocks and Their Assembly Into Complex Structures. *Nat. Mater.* **2007**, *6*, 557−562.
(3) Aizenberg, J.; Weaver, J. C.; Thanawala, M. S.; Sundar, V. C.; Morse, D. E.; Fratzl, P. Skeleton of Euplectella sp.: Structural Hierarchy from the Nanoscale to the Macroscale. *Science* **2005**, *309*, 275−278.
(4) Weiner, S.; Addadi, L. Design Strategies in Mineralized Biological Materials. *J. Mater. Chem.* **1997**, *7*, 689−702.
(5) Fratzl, P.; Weinkamer, R. Nature's Hierarchical Materials. *Prog. Mater. Sci.* **2007**, *52*, 1263−1334.
(6) Persson, P. V.; Hafren, J.; Fogden, A.; Daniel, G.; Iversen, T. Silica Nanocasts of Wood Fibers: A Study of Cell-Wall Accessibility and Structure. *Biomacromolecules* **2004**, *5*, 1097−1101.
(7) Zheng, Y.; Bai, H.; Huang, Z.; Tian, X.; Nie, F.-Q.; Zhao, Y.; Zhai, J.; Jiang, L. Directional Water Collection on Wetted Spider Silk. *Nature* **2010**, *463*, 640−643.
(8) Vukusic, P.; Sambles, J. R.; Lawrence, C. R. Structural Colour - Colour Mixing in Wing Scales of a Butterfly. *Nature* **2000**, *404*, 457−457.
(9) Mosauer, W. On the Locomotion of Snakes. *Science* **1932**, *76*, 583−585.
(10) Wainwright, S. A.; Vosburgh, F.; Hebrank, J. H. Shark Skin - Function in Locomotion. *Science* **1978**, *202*, 747−749.
(11) Keckes, J.; Burgert, I.; Fruhmann, K.; Muller, M.; Kolln, K.; Hamilton, M.; Burghammer, M.; Roth, S. V.; Stanzl-Tschegg, S.; Fratzl, P. Cell-Wall Recovery after Irreversible Deformation of Wood. *Nat. Mater.* **2003**, *2*, 810−814.
(12) Mattheck, C.; Kubler, H. *Wood—the internal optimization of trees*; Springer: Heidelberg, 1996.
(13) Trey, S. M.; Netrval, J.; Berglund, L.; Johansson, M. Electron-Beam-Initiated Polymerization of Poly(ethylene glycol)-Based Wood Impregnants. *ACS Appl. Mater. Interfaces* **2010**, *2*, 3352−3362.
(14) Kim, J.; Chung, S. E.; Choi, S. E.; Lee, H.; Kim, J.; Kwon, S. Programming Magnetic Anisotropy in Polymeric Microactuators. *Nat. Mater.* **2011**, *10*, 747−752.
(15) Shimomura, M.; Sawadaishi, T. Bottom-Up Strategy of Materials Fabrication: A New Trend in Nanotechnology of Soft Materials. *Curr. Opin. Colloid Interface Sci.* **2001**, *6*, 11−16.
(16) Truskett, V. N.; Watts, M. P. C. Trends in Imprint Lithography for Biological Applications. *Trends Biotechnol.* **2006**, *24*, 312−317.
(17) Ariga, K.; Nakanishi, T.; Michinobu, T. Immobilization of Biomaterials to Nano-Assembled Films (Self-Assembled Monolayers, Langmuir-Blodgett Films, and Layer-by-Layer Assemblies) and Their Related Functions. *J. Nanosci. Nanotechnol.* **2006**, *6*, 2278−2301.
(18) Oka, H.; Hojo, A.; Seki, K.; Takashiba, T. Wood Construction and Magnetic Characteristics of Impregnated Type Magnetic Wood. *J. Magn. Magn. Mater.* **2002**, *239*, 617−619.
(19) Zakaria, S.; Ong, B. H.; Ahmad, S. H.; Abdullah, M.; Yamauchi, T. Preparation of Lumen-Loaded Kenaf Pulp with Magnetite (Fe_3O_4). *Mater. Chem. Phys.* **2005**, *89*, 216−220.
(20) Small, A. C.; Johnston, J. H. Novel Hybrid Materials of Magnetic Nanoparticles and Cellulose Fibers. *J. Colloid Interface Sci.* **2009**, *331*, 122−126.
(21) Carrazana-García, J. A.; López-Quintela, M. A.; Rivas-Rey, J. Characterization of Ferrite Particles Synthesized in Presence of Cellulose Fibers. *Colloids Surf., A* **1997**, *121*, 61−66.
(22) Marchessault, R. H.; Rioux, P.; Raymond, L. Magnetic Cellulose Fibres and Paper: Preparation, Processing and Properties. *Polymer* **1992**, *33*, 4024−4028.
(23) Bayer, I. S.; Fragouli, D.; Attanasio, A.; Sorce, B.; Bertoni, G.; Brescia, R.; Di Corato, R.; Pellegrino, T.; Kalyva, M.; Sabella, S.; Pompa, P. P.; Cingolani, R.; Athanassiou, A. Water-Repellent Cellulose Fiber Networks with Multifunctional Properties. *ACS Appl. Mater. Interfaces* **2011**, *3*, 4024−4031.
(24) Olsson, R. T.; Samir, M.; Salazar-Alvarez, G.; Belova, L.; Strom, V.; Berglund, L. A.; Ikkala, O.; Nogues, J.; Gedde, U. W. Making Flexible Magnetic Aerogels and Stiff Magnetic Nanopaper Using Cellulose Nanofibrils as Templates. *Nat. Nanotechnol.* **2010**, *5*, 584−588.
(25) Katepetch, C.; Rujiravanit, R. Synthesis of Magnetic Nanoparticle into Bacterial Cellulose Matrix by Ammonia Gas-Enhancing in situ Co-Precipitation Method. *Carbohydr. Polym.* **2011**, *86*, 162−170.
(26) Speck, T.; Burgert, I.; Clarke, D. R.; Fratzl, P. Plant Stems: Functional Design and Mechanics. *Annu. Rev. Mater. Res.* **2011**, *41*, 169−193.
(27) Salmen, L.; Burgert, I. Cell Wall Features with Regard to Mechanical Performance. A Review COST Action E35 2004−2008: Wood Machining - Micromechanics and Fracture. *Holzforschung* **2009**, *63*, 121−129.
(28) Liu, Y. D.; Goebl, J.; Yin, Y. D. Templated Synthesis of Nanostructured Materials. *Chem. Soc. Rev.* **2013**, *42*, 2610−2653.
(29) Paris, O.; Fritz-Popovski, G.; Van Opdenbosch, D.; Zollfrank, C. Recent Progress in the Replication of Hierarchical Biological Tissues. *Adv. Funct. Mater.* **2013**, *23*, 4408−4422.
(30) Adachi, N.; Kuwahara, M.; Sia, C. K.; Ota, T. Porous Ba Ferrite Prepared from Wood Template. *Materials* **2009**, *2*, 1923−1928.
(31) Sia, C. K.; Sasaki, Y.; Adachi, N.; Ota, T. The Magnetic Properties of Porous Ni-Zn ferrites Prepared from Wood Templates. *Journal of the Ceramic Society of Japan* **2009**, *117*, 958−960.
(32) Pu, Y.; Zou, H.; Wang, J.-X.; Zhai, J.; Foster, N. R.; Chen, J.-F. Novel Sr−Zn−Co Hexagonal Ferrite Nano-Rods by Wood-Template Chemical Solution Synthesis. *Mater. Lett.* **2011**, *65*, 2213−2215.
(33) Schnepp, Z.; Yang, W.; Antonietti, M.; Giordano, C. Biotemplating of Metal Carbide Microstructures: The Magnetic Leaf. *Angew. Chem., Int. Ed.* **2010**, *49*, 6564−6566.
(34) Oka, H.; Hamano, H.; Chiba, S. Experimental Study on Actuation Functions of Coating-type Magnetic Wood. *J. Magn. Magn. Mater.* **2004**, *272−276* (Supplement), E1693−E1694.
(35) Jelinek, V. Precision A. C. Bridge Set for Measuring Magnetic Susceptibility of Rocks and its Anisotropy. *Studia Geophysica Et Geodaetica* **1973**, *17*, 36−48.
(36) Jelinek, V. Characterization of Magnetic Fabric of Rocks. *Tectonophysics* **1981**, *79*, T63−T67.
(37) Cornell, R. M., Schwertmann, U. *The Iron Oxides: Structure, Properties, Reactions, Occurences and Uses*, 2nd completely rev. and ext. ed.; Wiley-VCH: Weinheim, 2003.
(38) Laurent, S.; Forge, D.; Port, M.; Roch, A.; Robic, C.; Elst, L. V.; Muller, R. N. Magnetic Iron Oxide Nanoparticles: Synthesis, Stabilization, Vectorization, Physicochemical Characterizations, and Biological Applications. *Chem. Rev.* **2008**, *108*, 2064−2110.
(39) Massart, R. Preparation of Aqueous Magnetic Liquids in Alkaline and Acidic Media. *IEEE Trans. Magn.* **1981**, *17*, 1247−1248.
(40) Okada, H.; Sakata, K.; Kunitake, T. Formation of Oriented Iron Oxide Particles in Cast Multibilayer Films. *Chem. Mater.* **1990**, *2*, 89−91.
(41) Sedlář, M.; Matějec, V.; Grygar, T.; Kadlecová, J. Sol−Gel Processing and Magnetic Properties of Nickel Zinc Ferrite Thick Films. *Ceram. Int.* **2000**, *26*, 507−512.
(42) Nagata, T. *Rock Magnetism*; Maruzen Tokyo, 1961.
(43) Harris, E. E.; Kline, A. A. Hydrolysis of Wood Cellulose with Hydrochloric Acid and Sulfur Dioxide and the Decomposition of its Hydrolytic Products. *J. Phys. Colloid Chem.* **1949**, *53*, 344−351.
(44) Gierer, J. Chemistry of Delignification. *Wood Sci. Technol.* **1985**, *19*, 289−312.
(45) Kim, W.; Suh, C.-Y.; Cho, S.-W.; Roh, K.-M.; Kwon, H.; Song, K.; Shon, I.-J. A New Method for the Identification and Quantification of Magnetite−Maghemite Mixture Using Conventional X-Ray Diffraction Technique. *Talanta* **2012**, *94*, 348−352.

(46) de Faria, D. L. A.; Venâncio Silva, S.; de Oliveira, M. T. Raman Microspectroscopy of Some Iron Oxides and Oxyhydroxides. *J. Raman Spectrosc.* **1997**, *28*, 873−878.
(47) Jubb, A. M.; Allen, H. C. Vibrational Spectroscopic Characterization of Hematite, Maghemite, and Magnetite Thin Films Produced by Vapor Deposition. *ACS Appl. Mater. Interfaces* **2010**, *2*, 2804−2812.
(48) Shebanova, O. N.; Lazor, P. Raman Study of Magnetite (Fe_3O_4): Laser-Induced Thermal Effects and Oxidation. *J. Raman Spectrosc.* **2003**, *34*, 845−852.
(49) Long, J. W.; Logan, M. S.; Rhodes, C. P.; Carpenter, E. E.; Stroud, R. M.; Rolison, D. R. Nanocrystalline Iron Oxide Aerogels as Mesoporous Magnetic Architectures. *J. Am. Chem. Soc.* **2004**, *126*, 16879−16889.
(50) Shebanova, O. N.; Lazor, P. Raman Spectroscopic Study of Magnetite ($FeFe_2O_4$): A New Assignment for the Vibrational Spectrum. *J. Solid State Chem.* **2003**, *174*, 424−430.
(51) Hargraves, R. B.; Johnson, D.; Chan, C. Y. Distribution Anisotropy: The Cause of AMS in Igneous Rocks? *Geophys. Res. Lett.* **1991**, *18*, 2193−2196.
(52) Oka, H.; Fujita, H. Heating Characteristics of Magnetic Wood by Induction Heating. *IEEE Trans. Magn.* **1999**, *35*, 3520−3522.
(53) Oka, H.; Narita, K.; Osada, H.; Seki, K. Experimental Results on Indoor Electromagnetic Wave Absorber Using Magnetic Wood. *J. Appl. Phys.* **2002**, *91*, 7008−7010.
(54) Oka, H.; Kataoka, Y.; Osada, H.; Aruga, Y.; Izumida, F. Experimental Study on Electromagnetic Wave Absorbing Control of Coating-Type Magnetic Wood Using a Grooving Process. *J. Magn. Magn. Mater.* **2007**, *310*, e1028−e1029.
(55) Oka, H.; Terui, M.; Osada, H.; Izumida, F.; Namizaki, Y. Controlling Electromagnetic Wave Absorption Characteristics by Changing Mixing Ratios of Magnetic Powder of Powder-Type Magnetic Wood. *INTERMAG Asia 2005: Digest of the IEEE International Magnetics Conference (IEEE Cat. No.05CH37655)*; 2005; pp 1099−100.
(56) Oka, H.; Tanaka, K.; Osada, H.; Kubota, K.; Dawson, F. P., Study of Electromagnetic Wave Absorption Characteristics and Component Parameters of Laminated-Type Magnetic Wood with Stainless Steel and Ferrite Powder for Use as Building Materials. *J. Appl. Phys.* **2009**, *105*.
(57) Oka, H.; Terui, M.; Osada, H.; Sekino, N.; Namizaki, Y.; Oka, H.; Dawson, F. P. Electromagnetic Wave Absorption Characteristics Adjustment Method of Recycled Powder-Type Magnetic Wood for Use as a Building Material. *IEEE Trans. Magn.* **2012**, *48*, 3498−3500.